Reliability Engineering and System Safety 209 (2021) 107447

Contents lists available at ScienceDirect

Reliability Engineering and System Safety

journal homepage: www.elsevier.com/locate/ress

Quantification of the resilience of integrated energy systems using dynamic simulation

Anne Senkel *, Carsten Bode, Gerhard Schmitz

Hamburg University of Technology, Institute of Engineering Thermodynamics, Denickestraße 15, 21073 Hamburg

ARTICLE INFO

Keywords:
Resilience Assessment
Modelica
Dynamic Simulation
Integrated Energy System

ABSTRACT

This paper demonstrates the use of dynamic simulation to model and assess the resilience of an integrated energy system. First, several approaches from the field of resilience assessment are evaluated, and the most suitable is chosen and adapted to develop a metric that is applicable to dynamic simulation results. Second, as proof of concept, a model of an integrated energy system (gas, heat and power sector) is presented and evaluated using the introduced metric. To demonstrate how changes in the system architecture influence the resilience, two modifications are tested. It can be shown that the metric is suitable to quantify the resilience of an integrated energy system and assess suggestions for improvements. Therefore, it can also be added and compared to other quantitative metrics such as CO_2 emissions or costs.

1. Introduction

The consequences of ongoing climate change highlight the need for CO_2 mitigation, and thus a deep structural transformation of our energy supply system [1,2]. Since renewable energies vary in time and local occurrence, innovative technologies such as integrated energy systems, energy storage and demand-side-management are evolving. This leads to new and complex energy systems, which need to be assessed and investigated regarding their economic efficiency, sustainability and reliability. Because of the high complexity and critical nature of these systems, the call for resilience assessment rather than traditional risk analysis has recently emerged [3].

Additionally, the increase in unlikely yet high-impact events as 9/11 or the Fukushima Hamadōri earthquake and their related consequences has driven this progress. In contrast to traditional risk management, the consideration of resilience allows the evaluation of complex systems and the preparation for unforeseen disturbances [3]. In this context, models of energy systems can contribute by assessing not only CO_2 emissions and cost, but also the resilience of an energy system.

The word resilience originates from the Latin word “resilire” which means “to jump back, to rebound”. In the past, the concept of resilience has emerged in various research fields, such as material science, the judicial system and psychology [4]. In the 1970s, the ecologist C. S. Holling used the term to describe the behavior of ecosystems. His first approach to resilience, which he later referred to as engineering resilience, defines resilience as a “measure of persistence of systems and of their ability to absorb change and disturbance” (Holling, 1973, p.14 [5]). He later developed a more dynamic consideration of resilience measured “by the magnitude of disturbance that can be absorbed before the system changes its structure” (Holling and Gunderson, 2002, pp. 27-28, [6]). This second approach was defined as ecosystem resilience. While the first is derived from a very mechanical understanding of stability, the latter examines conditions beyond a stable state of equilibrium. [6]

The general concept of resilience considers sociological and technological issues, combining two very disparate research fields. Since this paper discusses the implementation of resilience in dynamic simulations of energy systems, resilience is approached from an engineering point of view. The assessment methods presented in this paper therefore only evaluate the technical component of resilience, and must be regarded as just one part of a holistic resilience assessment. For more information on the socio-technological assessment of resilience, please refer to Linkov and Palma-Oliveira [3].

While interest in the research field of resilience is not only increasing in energy analysis, the development of a standardized assessment method is still ongoing. Hosseini et al. and Gasser et al. provide an overview of the current development of frameworks for the assessment of resilience [7,8]. In the following, only those assessment methods, which focus on the quantification of resilience of critical infrastructure, are presented.

* Corresponding author.
E-mail address: anne.senkel@tuhh.de (A. Senkel).

https://doi.org/10.1016/j.ress.2021.107447
Received 12 June 2020; Received in revised form 30 November 2020; Accepted 2 January 2021
Available online 4 January 2021

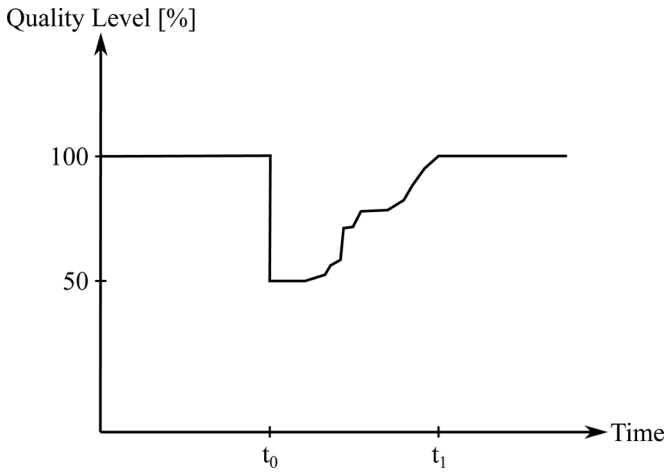

Fig. 1. The resilience triangle as a measure of resilience according to [9]

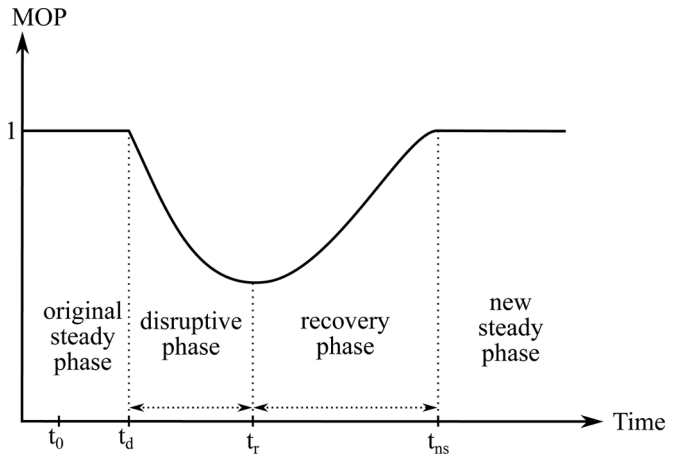

Fig. 2. Typical curve of the MOP according to [12]

A concept, which is often referred to is the so-called resilience triangle, which was introduced by Bruneau et al. in [9]. It is based on the observation that disruptive events cause abrupt changes in the performance quality Q, and gradual recovery to the original performance quality level (see Fig. 1). The resilience R of a system is thus defined as:

$$R = \int_{t_0}^{t_1} 100\ \% - Q(t)dt \tag{1}$$

This approach is also used by Cimellaro et al. to quantify disaster resilience [10]. Francis and Bekera decompose the resilience triangle by evaluating the recovery speed and comparing the system's functionality prior to, during and after the disturbance [11]. This approach is further developed by Nan and Sansavini who introduce a method to evaluate the capabilities of resilience in more detail [12]. Goldbeck et al. also use a performance-based approach to assess the interdependence of urban infrastructure systems using dynamic network flow models [13]. Toroghi and Thomas develop a framework for the resilience analysis of electric infrastructure systems with a special focus on ancillary systems [14].

In this paper, we adapt Nan and Sansvini's approach to the specifics of dynamic simulations of integrated energy systems (Section 2). To test the applicability of this method, we present an artificial energy system and two related resilience intervention plans (Section 3). In Section 4, we discuss and evaluate the results using the presented method. Section 5 presents concluding remarks and recommendations for future work.

2. Methods

2.1. Resilience Assessment according to Nan and Sansavini

As an alternative to the abstract variable performance quality Q, Nan and Sansavini introduce the Measure of Performance MOP [12]. As a suitable MOP, they propose e.g. the ratio between actually delivered and demanded total power in an electric transmission system or the ratio between currently available transmission lines and total transmission lines. Therefore, the MOP ranges between 0 (total performance loss) and 1 (normal performance). A typical curve of such an MOP is depicted in Fig. 2.

With this definition, an MOP above 1 shows a system performance above normal operation, and thus an improvement in comparison to normal operation. This behavior can be observed when system recovery measures during a disturbance lead to an enhancement beyond the recovery phase, e.g. installing additional diesel power generators to bridge a malfunctioning transmission line, resulting in a higher redundancy of the power grid after the transmission line is fixed.

In their resilience assessment, Nan and Sansavini describe the absorptive, adaptive, restorative and recovery capability of the considered system each by measurable characteristics of the system's response to disruption. To identify the absorptive and adaptive capacity, they introduce the measure Rapidity, i.e. the average slope of the MOP:

$$RAPI = \frac{\Delta MOP}{\Delta t} \tag{2}$$

The ratio of Rapidity during the recovery and the disruptive phase is later implemented into the resilience metric GR.

Nan and Sansavini characterize the absorptive capacity of the system further by measuring its Robustness:

$$R = \min(MOP) \tag{3}$$

Moreover, they combine absorptive, adaptive and restorative capability in the Performance Loss, the area bounded by the MOP curve:

$$PL = \int_{t_d}^{t_{ns}} (MOP(t_0) - MOP(t))dt \tag{4}$$

This measure equals the area of the previously-mentioned resilience loss triangle and is divided by the recovery time to gain a time-averaged value:

$$TAPL = \frac{\int_{t_d}^{t_{ns}} (MOP(t_0) - MOP(t))dt}{t_{ns} - t_d} \tag{5}$$

Finally, Nan and Sansavini introduce the measure Recovery Ability to mirror the system's recovery capacity:

$$RA = \frac{|MOP(t_{ns}) - MOP(t_r)|}{|MOP(t_0) - MOP(t_r)|} \tag{6}$$

Finally, they combine the Robustness, Rapidity, Performance Loss and Recovery Ability into the resilience metric GR:

$$GR = R \cdot \frac{RAPI_{RP}}{RAPI_{DP}} \cdot TAPL^{-1} \cdot RA \tag{7}$$

With this definition, the lowest value of GR is zero, representing a non-resilient system while there is no upper limit for GR.

2.2. Adaptions to Nan and Sansavini

In the gas and heat sector, a medium provides energy by flowing through pipelines. In the power sector, the energy transport is based on charge exchange and thus not bound to a moving fluid. Therefore, the time frames and system behaviors of these sectors largely differ. However, for the resilience assessment, the authors needed to find values for each sector that represent their respective performance. Hence, we chose the demanded energy flow of each consumer in the system, since

the main purpose of every energy supply system is to provide its consumers with the required energy at the corresponding time of demand. This leads to neglecting certain influences and effects in the power sector on the final Resilience Index. For example, an electric power system already encounters serious difficulties when its frequency or voltage show instabilities even though no load is reduced yet. These effects could also be modeled and evaluated using the models presented in this paper. Focusing on the transferred energy flows allows the comparability of three very different energy sectors and thus the evaluation of an integrated energy system. For a more detailed consideration of the power sector's resilience in combination with dynamic simulation, we recommend Heckel and Becker [15].

Nan and Sansavini propose to evaluate the chosen measure as MOP by setting it in relation to the measure when the system is undisturbed. Nonetheless, in energy systems the case may occur that the demanded energy flow is zero (e.g. at night, over weekends or due to control mechanisms), resulting in an indeterminable MOP. Therefore, we do not put the demanded energy flow into any ratio before assessing it. Nevertheless, to gain a dimensionless figure we normalize each of the following elements of the resilience value with a suitable normalization value. To avoid any misunderstanding, we further refer to the demanded energy flow as x and to the measure of performance introduced by Nan and Sansavini as MOP.

Nan and Sansavini assume a general curve behavior of the MOP as depicted in Fig. 2. However, when looking into the heat sector, one can observe that the characteristic response of the energy demand of heating systems follows the graph shown in Fig. 3. Here, a malfunctioning of the heat sector leads to the cooling down of the heating system and the affected buildings. This leads to a reheating phase after the correction of the defects. In this phase, x exceeds its undisturbed value and behaves different to the MOP. Therefore, we adapted the method of Nan and Sansavini [12] as follows.

In the heat and gas sector in particular, slight deviations from the set point of the energy demand are tolerable, since these sectors normally possess buffering capacities which dampen the effects of minor deviations. Thus, we introduce a tolerance band in which deviations of the considered measures are judged as tolerable and hence have no effect on the resilience assessment. An example of a tolerance band is depicted in Fig. 4.

As shown before, in the heat sector, the slope of x becomes both positive and negative, several times. In these cases, the Rapidity RAPI provides only limited information about the system's behavior. On that account, we replace it with the Recovery Time RT:

$$RT = \frac{t_{ns} - t_d}{\Delta t_{norm}} \tag{8}$$

As normalization time Δt_{norm}, the authors propose the duration of the induced disturbance (c.f. Fig. 4).

For the Robustness R, we suggest transferring it to the Maximum

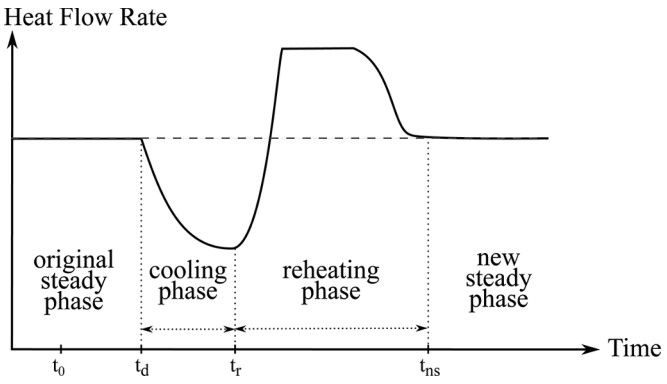

Fig. 3. Typical recovery curve of a heating system

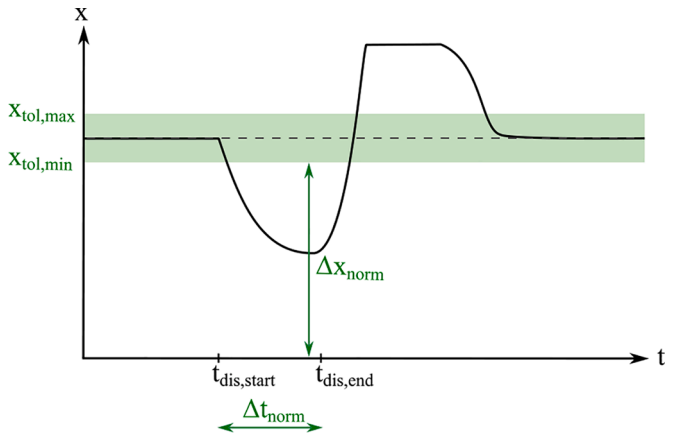

Fig. 4. Exemplary tolerance band and normalization values

Deviation MD of the considered energy flow:

$$MD = \frac{\Delta x_{max}}{\Delta x_{norm}} \tag{9}$$

With Δx as the deviation outside of the tolerance band (c.f. Fig. 4):

$$\Delta x = \begin{cases} x - x_{tol,max} & \text{if} \quad x \geq x_{tol,max} \\ 0 & \text{if} \quad x_{tol,\ min} < x < x_{tol,max} \\ x_{tol,min} - x & \text{if} \quad x \leq x_{tol,min} \end{cases} \tag{10}$$

This has the benefit that higher values of MD indicate a less resilient system behavior, which is also true for the other two elements. As the normalization value, we use the maximum possible deviation at the time of maximum deviation (c.f. Fig. 4).

We integrate the concept of the Performance Loss into our resilience assessment by normalizing it with $A_{norm} = \Delta x_{norm} \cdot \Delta t_{norm}$:

$$PL = \frac{\int_{t_d}^{t_{ns}} \Delta x dt}{A_{norm}} \tag{11}$$

While the values of the Maximum Deviation and the Recovery Time do not necessarily correlate, the Performance Loss often corresponds to these two values. However, this element still provides additional information about the system's behavior during the disruptive and recovery phase. Fig. 5 depicts two systems with identical Maximum Deviation and Recovery Time. The first system recovers very abruptly and after a certain amount of time, whereas the second system recovers gradually and right after reaching its minimal performance. By using the Performance Loss, we are able to differentiate these recovery behaviors in our resilience value.

Considering Nan and Sansavini's Recovery Ability makes only sense under the condition that exceeding the undisturbed value means an improvement of the system's performance. As shown in Fig. 3, this may also occur during reheating phases as part of the system's recovery. Therefore, the authors did not implement this measure into their Resilience Index.

Since the resilience measures used for this paper differ from those used by Nan and Sansivini, and in order to define an upper limit of the resilience metric, we propose the following definition of a Resilience Index:

$$RI = \frac{1}{1 + RT \cdot MD \cdot PL} \tag{12}$$

Since high values of Recovery Time, Maximum Deviation and Performance Loss reflect a less resilient system behavior, we integrate them in the denominator. Adding one to their product leads to the following limits of RI:

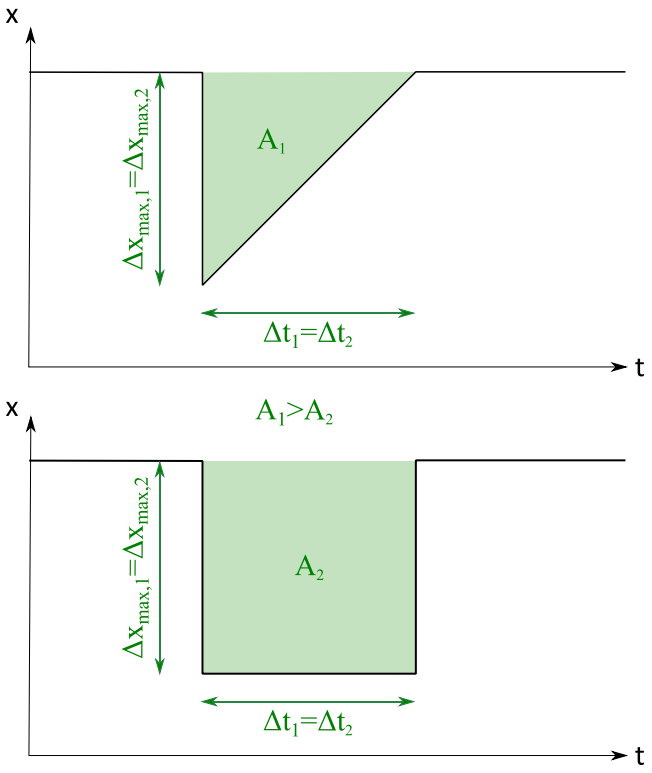

Fig. 5. Example of two system behaviors with identical Maximum Deviation and Recovery Time but different Performance Loss

- RI = 1 … the value considered shows only tolerable deviations when the system is disturbed. The system's functionality is not negatively affected by the investigated disturbance.
- RI = 0.5 … the value considered shows a total loss of performance for the duration of the disturbance. After the end of the disturbance, the system is able to restore its functionality immediately.
- RI = 0 … the value considered does not return to the tolerated deviation range. The system is not able to restore its functionality in the simulated time period.

This resilience index can be calculated for every consumer in the energy system considered. To gain an overall view of the resilience of the individual energy sectors, the resilience indices of their consumers (RI_c) are weighted by their demand during the time period considered E_c and combined into one sector resilience index RI_{sec} as follows:

$$RI_{sec} = \sum_c \frac{E_c}{E_{sec}} \cdot RI_c \tag{13}$$

This adapted resilience assessment method can now be used to evaluate the simulation results of integrated energy systems.

2.3. Dynamic Simulation

In the next section, we present an artificial but representative integrated energy system which we built using models from the open-source TransiEnt Library [16,17], which was developed to dynamically model integrated energy systems with high shares of renewables. The models are based on the non-proprietary, object-oriented, equation-based modeling language Modelica [18], which allows the coupling of models from various domains. Therefore, the integration of models from the heat, gas and power sector into one simulation is possible. The modeling is either based on physical fundamentals or characteristic curves and was validated accordingly, when possible and reasonable [16,17]. Since the presented energy system is artificial, validation with experimental data is not possible. However, all results were verified in terms of their plausibility. The authors used Dymola [19] as simulation environment.

3. Model Description

3.1. Reference System

The energy system modeled incorporates the gas, heat and power sector, including producers, consumers and storage and control units in each sector (Fig. 6). The authors wish to emphasize that they integrated some flaws into the structure of the systems presented, regarding their reliability and economic efficiency. This was done because the purpose of this system is not to depict a real energy system, but rather to prove the applicability and specifics of the resilience index. The key parameters of the modeled components are listed in Table 1.

The gas sector consists of eight pipelines which form a loop, so that there is redundancy. The pipe, in which we will later introduce the disturbance investigated, is part of the loop. This pipe is split into two parts for numerical reasons. The models of the pipelines and junctions use discretized dynamic mass and isothermal energy balances, and include a physical pressure loss calculation. The medium data is provided by the TILMedia library [20]. The total length of the pipelines is 47 km and the volume is 4,400 m^3.

The gas is fed into the grid by a gas source in the southwest. There are three gas consumers supplied by the grid: an industrial consumer in the northwest (NW), and two residential areas which burn the gas in boilers for heating purposes in the northeast (NE) and southeast (SE). Furthermore, a combined cycle power (CCP) plant uses natural gas to produce power in a gas and steam cycle. The usable excess heat of the steam cycle is used to provide heat for a district heating network (DHN). Therefore, the CCP plant couples the gas sector with the heat and power sector. Another coupling technology is the electrolyzer in the southwest of the gas grid. This plant produces hydrogen, which is fed into the gas grid at times of high renewable power production. All gas consumers can take gas from the grid as long as the pressure at the corresponding transfer station is above a given minimum pressure.

The heat sector in the model consists of three sections: two residential areas that are provided with heat by gas boilers, and one residential area where the households are connected to the district heating network supplied by the CCP plant.

The reaction of a heating system to disruptions depends significantly on the thermal properties of the houses supplied, as well as environmental effects such as outside temperature, solar radiation or wind speed. However, modeling all these effects in detail for every house requires extensive computational effort. Hence, the authors used a reduced-order approach to model all three housing areas [21]. We aggregated the thermal processes, and thus calculated the heat demand of a house with a reduced number of heat capacitors and conductors. For every section, we modeled one characteristic house following this method.

The physical model is connected to the DHN or gas boiler by a heat flow multiplier. This connector scales up the heat flow rate between the connected models. Therefore, the connected heating system supplies the heat demand of several thousand households, while the model of the single house is only supplied with the corresponding fraction of the overall heat flow rate produced. With this approach, we were able to integrate the characteristic behavior of an average household into an integrated energy system model, while avoiding extensive computational effort.

Please note that the research in this field is ongoing, and dynamic models with higher spatial discretization and acceptable computational effort are currently under investigation [22]. Since this paper does not focus solely on the heat sector, the authors did not implement these approaches. However, the object-orientation of Modelica enables subsequent coupling with a more detailed model of the residential heating

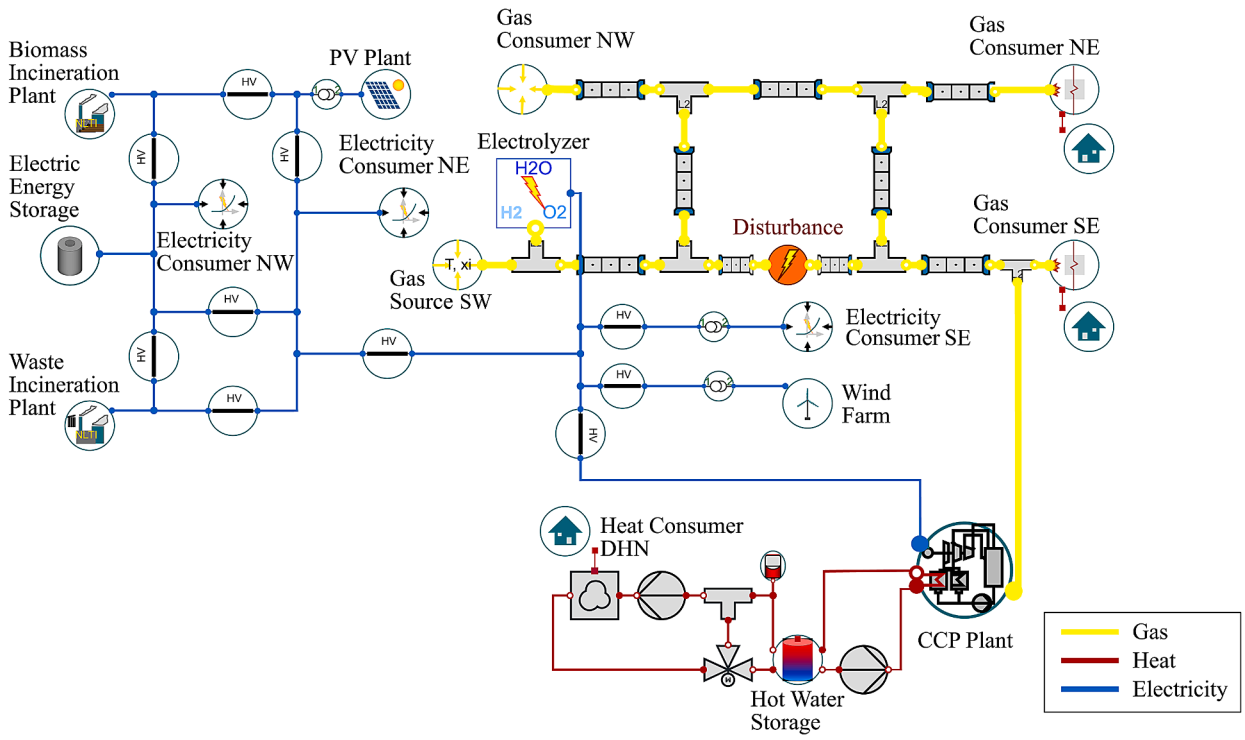

Fig. 6. Structure of the energy system investigated (Reference System)

Table 1
Key parameters of the energy system's components

Parameter	Value
Gas sector	
Feed-In Pressure at Gas Source	12.5 bar
Minimum Pressure Gas Boiler	2 bar
Minimum Pressure CCP Plant	2 bar
Total Length of the Pipelines	47 km
Volume of the Gas Grid	4400 m^3
Heat Sector	
Number of Households NE	58 100
Number of Households SE	29 050
Number of Households DHN	6 260
Nominal Heat Flow Rate Gas Boiler NE	280 MW
Nominal Heat Flow Rate Gas Boiler SE	140 MW
Nominal Heat Flow Rate CCP Plant	30 MW
Volume of Buffer Storage DHN	1 720 m^3
Supply Temperature DHN	80°C
Nominal Mass Flow Rate DHN	240 kg/s
Nominal Power Electric Boiler	140 MW
Power Sector	
Nominal Power Biomass Plant	80 MW
Nominal Power Waste Incineration Plant	100 MW
Nominal Power Wind Farm	60 MW
Installed PV Plant Area	10 500 m^2
Nominal Electric Power CCP Plant	60 MW
Nominal Power Electrolyzer	1 MW
Maximum Discharge Rate Electric Energy Storage	50 MW
Maximum Charge Rate Electric Energy Storage	70 MW
Storage Capacity Electric Energy Storage	6 GWh
Proportional Load Factor NW	2.6
Proportional Load Factor NE	2.5
Proportional Load Factor SE	0.8

demand.

In the district heating network, a hot water storage is included which can cover the heat demand for two hours in case of a CCP plant shutdown at design conditions. The model for the storage uses a discretized dynamic energy balance to take into account the effects of the stratification within the storage. The heat flow rate of the CCP plant is controlled to achieve a water temperature of 85°C at the top of the buffer storage. The supply temperature of the DHN is regulated by a backmixing unit, depending on the outside temperature, following a heating curve with a maximum temperature of 80°C. For the ambient temperature, we used the temperature curve of 2012 measured in Hamburg, Fuhlsbüttel [23]. The heat flow rate to all three typical households is controlled to achieve a room temperature of 22°C according to EN 15251 [24].

In the electric grid, we implemented three consumers whose demand is modeled according to standard load profiles for industry (northwest, NW), agriculture (northeast, NE) and households (southeast, SE) [25]. The dynamic behavior of the loads is modeled according to [26]. In this model, the load reacts linearly to the frequency. The proportional factors for the consumers are taken from [26] and listed in Table 1. For the agricultural load, we assumed a distribution of 50 % power for heating, 25 % for electric motors and 25 % for electronics [27], which results in a proportional factor of 2.5.

The power demanded is produced by wind turbines, photovoltaic (PV) plants, a biomass power plant, a waste incineration plant and the previously-mentioned CCP plant. The operation of the CCP plant is determined by the heat demand of the DHN and the power demand in the electric grid. As long as both values are within the operating range of the CCP plant (c.f. Fig. 7), both demands can be satisfied. If one of the boundaries shown is reached, the electric power output or the heat flow rate is limited.

Furthermore, we implemented an electric energy storage to absorb possible surpluses of electric energy and avoid curtailment of the renewables. Therefore, the production of the wind turbines and the PV plants only depends on the current solar and wind conditions. The merit order, in which the other plants are used, is defined as follows: discharging of the storage – CCP plant – biomass plant – waste incineration plant. Production is controlled according to the grid frequency and thus the current supply and demand in the grid. The models for the transmission lines are quasi-stationary and allow the computation of voltage

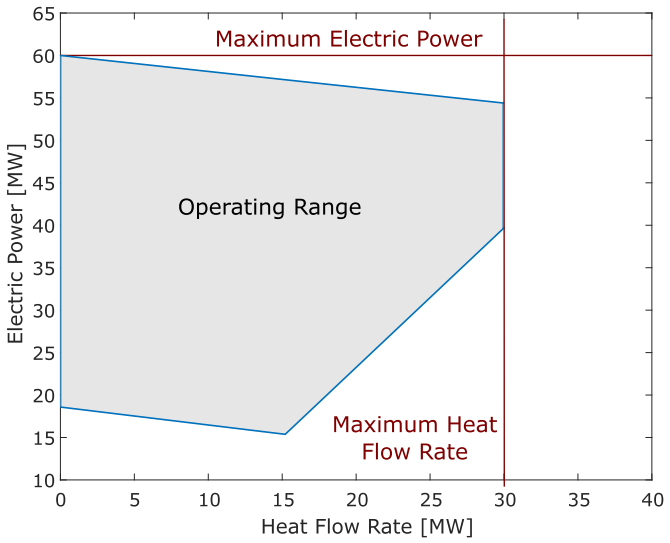

Fig. 7. Operating range (blue) of the CCP plant

drop and power loss.

To assess the resilience of the system presented (Reference System), we chose a full pipeline closure in the south as a disruption. In reality, this might occur when a component or control unit malfunctions or a gas pipeline ruptures. The duration of the disturbance was set to 14 hours, the timespan of interrupted gas supply due to the Baumgarten incident in December 2017 [28]. As the start of the pipeline closure, we chose 3:45 am on February 4th since the coldest annual temperatures appear in this period and consequently the heating system is the most vulnerable.

3.2. Resilience Intervention Plans

Later on, we will discuss two system changes to enhance the system's resilience to the disturbance considered (c.f. Fig. 8). Both are deemed as alternative ways of providing heat to the customers of the DHN (Resilience Intervention Plan 1, RIP 1) or the customers in the southeast (Resilience Intervention Plan 2, RIP 2). While the first is expected to improve the system's resilience by increasing its decentralization, the second raises the redundancy of the heat system.

The first change is the installation of a second CCP plant in the southwest of the gas grid, which provides the western part of the district heating grid with heat and also feeds into the electric grid. Therefore, the nominal power of the two CCP plants each equals half of the power of the CCP plant in the Reference System. Furthermore, the district heating grid is split in half, and each network is supplied by one of the CCP plants. In the following, we refer to this system as RIP 1.

As second intervention, we studied the effects of electric boilers as backup heat suppliers in the housing area in the southeast. For this purpose, we connected the heat Consumer SE to an electric boiler. This boiler is also supplied by the electric grid. Its nominal heat flow rate corresponds to that of the gas boiler. When the gas boiler fails to supply the households with heat, the electric boilers are turned on. We refer to this system as RIP 2.

While RIP 1 is an intervention at the central heat provider of the DHN, RIP 2 changes the decentral heat supply of each household in the southeast. We expect both systems to not only have an impact on the behavior of the heat sector but also the power and gas sector.

For the power sector, we anticipate different consequences. In RIP 1, the number of undisturbed power plants and hence the available power production during the disturbance is increased. In contrast to this, in RIP 2, the power load during the disturbance is additionally increased by the operation of the electric boilers. Thus, the first intervention should influence the power system in a positive way while the second is expected to have negative consequences.

For the gas sector, we expect improvements in the phase after the disturbance for both interventions since the households should recover more quickly and therefore should need less gas for reheating. For a successful proof of applicability, the systems' responses to the induced disturbance need to be reflected in their resilience indices.

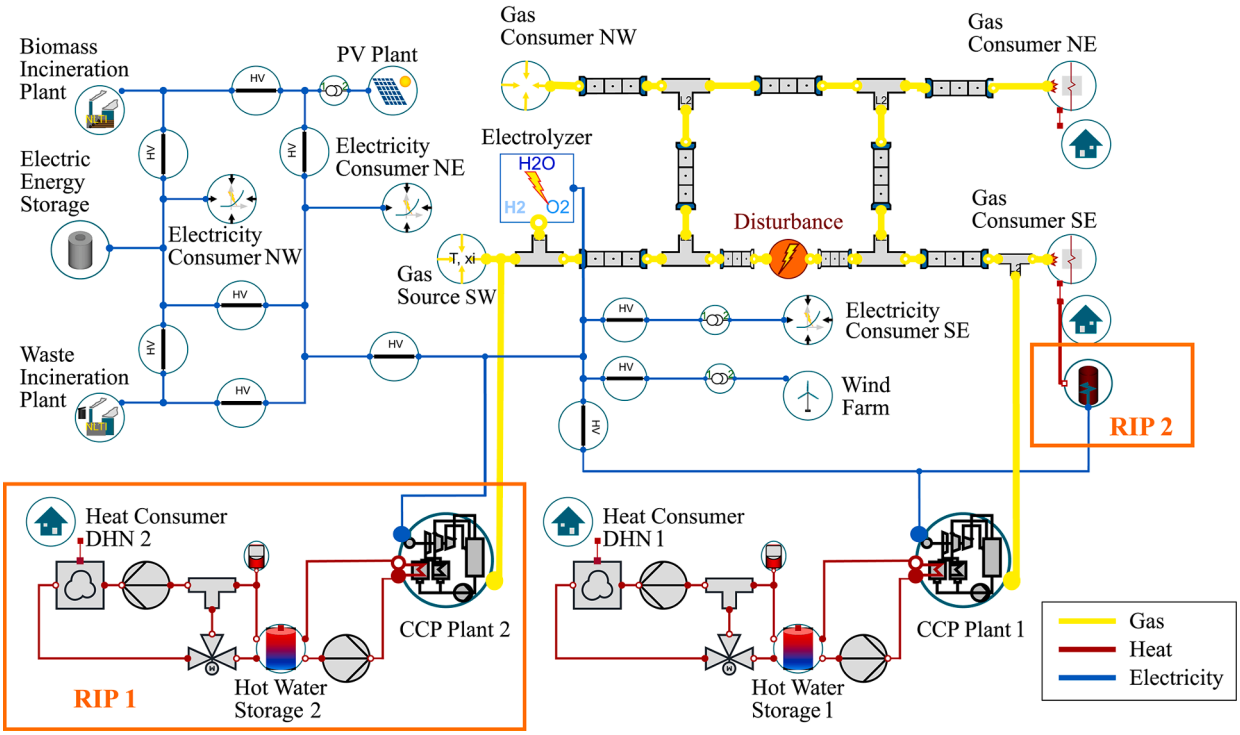

Fig. 8. Resilience Improvement Plans 1 and 2

4. Results

In the following section, we describe the disturbance and recovery behavior of the three systems examined. For this purpose, we present the simulation results of the dynamic models for a disturbed (dashed line) and undisturbed (solid line) system in Figs. 9, 10 and 11. For a better understanding of the systems' behavior, the curves of gas pressure, room temperature and net frequency are depicted. For the subsequent resilience assessment, the energy flows of each system and sector are investigated, which are: enthalpy flow rate (gas sector), heat flow rate (heat sector) and electric power (power sector). Thus, their curves are charted as well.

4.1. Reference System

In the reference scenario, the consequences of the pipeline closure are not only visible in the gas sector but also in the heat and power sector. Since the gas and thus the energy supply of the consumers in the southeast is cut, the gas boilers and the CCP plant in this area are shut down. This leads to shortages in the heat and power supply that also have negative effects on room temperature and net frequency.

In the gas sector, one can see that the consumers in the north are not negatively affected by the pipeline closure. The gas pressure at their transfer stations decreases after the closure but is sufficiently high to satisfy their gas demand. Ergo, the curves of their enthalpy flow rate for the disturbed and undisturbed system match.

For the gas consumers in the southeast, the main supply pipeline is shut. Therefore, the pressure at their gas transfer stations drops below the minimum operating pressure of 2 bar (c.f. Fig. 9, a), and is too low to allow normal operation. Consequently, their controllers turn the boilers off during the disturbance. The same is the case for the CCP plant which is shut down as well. These shutdowns lead to a smaller gas demand and accordingly to a short-term pressure increase. Nonetheless, the gas pressure remains at around 8 bar and is not restored to its undisturbed value of about 10 bar until the pipeline is fixed. After the disturbance, the consumers are switched on again by their controllers with an hour's delay. Hence, the pressure increases slightly after the end of the disturbance, when the gas grid is already operating normally, but not all gas consumers are taking gas from the grid yet.

After the pipeline is restored, the gas demand of the consumers in the southeast and thus their enthalpy flow rate is higher than in the undisturbed simulation (c.f. Fig. 9, b), since the cooled down houses need to be reheated. The gas demand of the CCP plant, however, returns directly to the original level. Here, the reheating process is not reflected in the enthalpy flow rate, since the gas is mainly used to supply power to the electric grid. During the reheating of the DHN, the power output of the plant decreases to provide additional heat for the DHN. The resulting shift of the operation point leads to an increase in the total efficiency of the plant from 0.87 in the undisturbed system to 0.93 in the disturbed system during reheating, resulting in almost the same enthalpy rate as in the undisturbed case. Both operation points are depicted in Fig. 12. Note that the heat flow rate in both simulations depends on the heat demand of the DHN. Therefore, in the undisturbed system, the heat flow rate varies slightly due to changing ambient temperatures, leading to a larger operational area than in the disturbed case where the DHN demands the maximum heat flow rate over the whole reheating process. We also observed this behavior for the CCP plants in RIP 1 and 2.

The heat flow rates of the housing areas in the east behave analogically to the enthalpy flow rates (Fig. 9, d). In the northeast, the gas supply is not disturbed, leading to an undisturbed heat supply as well. The room temperature of those households can be maintained at 22°C (Fig. 9, c).

In the southeast, the heat flow rate becomes zero after the shutdown of the gas supply. The room temperature accordingly drops to a minimum of 16.7°C. Only when the gas supply of the gas boiler is restored, does the room temperature rise again. During the subsequent reheating phase, the heat flow rate to the consumers exceeds the undisturbed curve after the disturbance.

For the DHN, the buffer storage has a noticeably positive effect. Since it is able to provide heat even after the CCP plant is shut down, the room temperature of the corresponding households only declines gradually. However, since the hot water storage cools down as well, the supply temperature of the DHN system stays below its set point for several hours after the CCP plant is turned on again. Therefore, the temperature curves of the DHN and Consumer SE almost match during the reheating phase, even though the drop in room temperature of the DHN is not as strong as the one for Consumer SE.

In the power sector, the other producers in the sector are able to increase their production and therefore dampen the effects of the shutdown of the CCP plant. Nevertheless, the production is not sufficient to meet the demand. Hence the grid's frequency drops significantly (Fig. 9, e), leading to an insufficient coverage of the load of Consumer NW and NE during their peak demand (Fig. 9, f).

4.2. Resilience Intervention Plan 1

In RIP 1, we observe similar consequences in the gas sector due to the pipeline closure as in the reference system. However, the splitting of the CCP plant allows the sufficient supply of half of the DHN customers and one of the CCP plants which ensures a sufficient supply of all electric customers.

In the gas sector, splitting the CCP plant in two also cuts the enthalpy flow rate to the CCP plant into halves (Fig. 10, b). While the original CCP plant in the east still encounters a shutdown of its enthalpy flow rate, the gas supply of the CCP plant in the west is not disturbed.

Additionally, the splitting has a positive effect on the gas consumer in the southeast. Since the CCP plant in the east is smaller than in the Reference System, its gas mass flow rate is lower, leading to higher pressure at the gas transfer station in the southeast (Fig. 10, a). Therefore, the minimum pressure of the gas consumer in the southeast is reached later, and the gas and heat supply can be maintained for a longer time. However, the time scale of this delay only encompasses 18 minutes.

As expected, the heat flow rate and room temperature of the undisturbed western part of the DHN meet their set points (Fig. 10, c-d). Since the gas flow to the other consumers in the gas grid is barely affected, the curves of the other heat flow rates and room temperatures also only change slightly in comparison to the Reference System. Additionally, one can see that the splitting process also causes halved heat flow rates to the district heating networks.

In the power sector, the failure of a now smaller CCP plant and the existence of another CCP plant helps to maintain the power production. Hence, the demand of Consumer NW and NE is now met, even at their peaks (Fig. 10, f). Thus, the net frequency can be maintained at 50 ± 0.03 Hz (Fig. 10, e), indicating a more stable operation of the electric grid than in the Reference System.

4.3. Resilience Intervention Plan 2

Due to the installation of the electric boilers in RIP 2, the heating demand of the customers in the southeast can be met at all times. This decreases the necessary enthalpy flow rate of this area after the disturbance. Due to the high demand of electric power, the electric grid is destabilized and not able to provide sufficient power to all customers.

In the gas grid, the installation of the electric boilers only affects its enthalpy flow rate after the disturbance. Since the electric boilers maintain the heat supply of the households, no additional gas flow is needed for reheating after the disturbance. Thus, the enthalpy flow rate returns to the undisturbed curve immediately after the gas boilers are turned on again (Fig. 11, b). The other gas consumers are not affected by the electric boilers' operation.

In the heating sector, the room temperature of Consumer SE can be

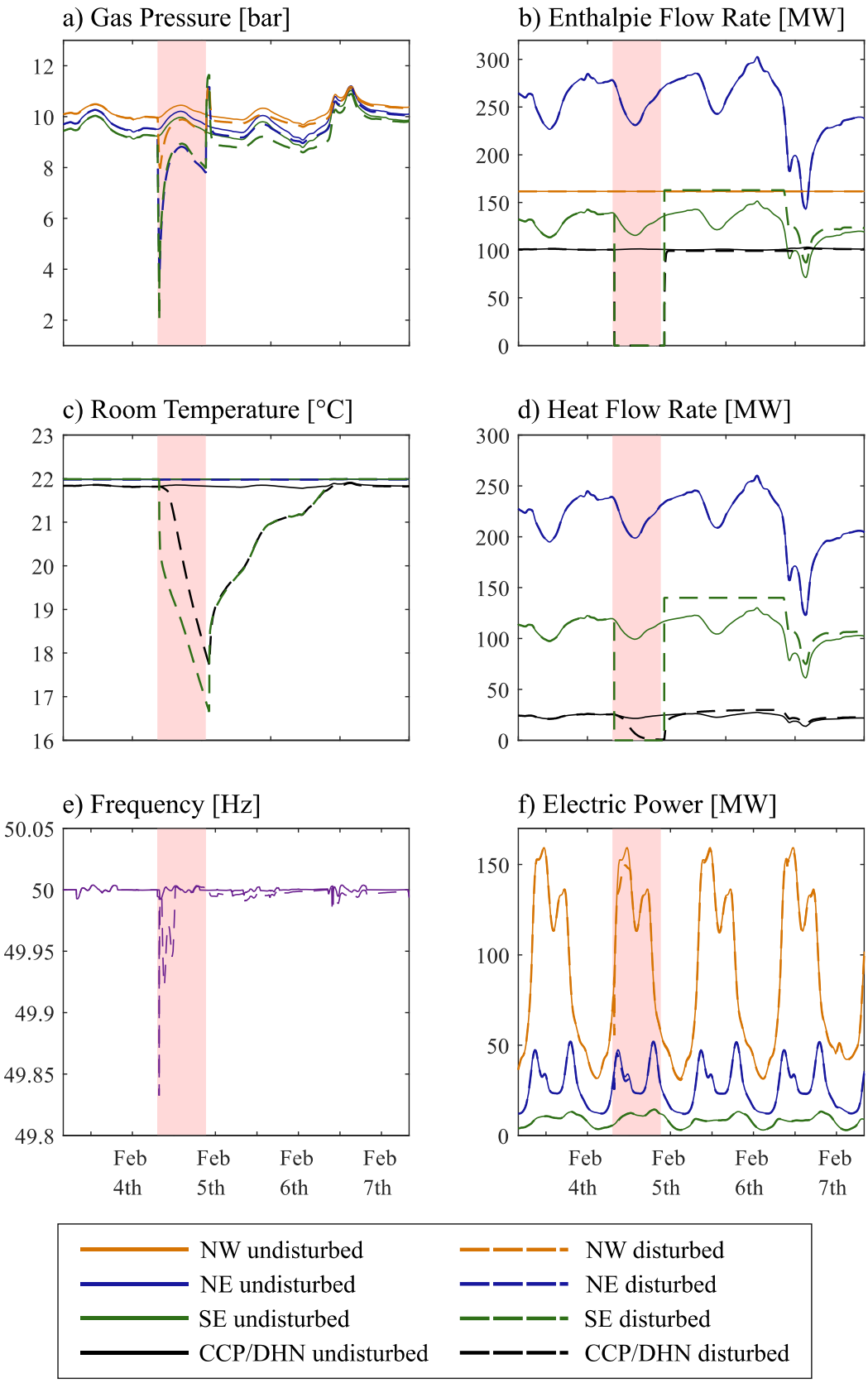

Fig. 9. Simulation results of characteristic values of the gas, heat and power sector for the undisturbed (solid line) and disturbed (dashed line) Reference System

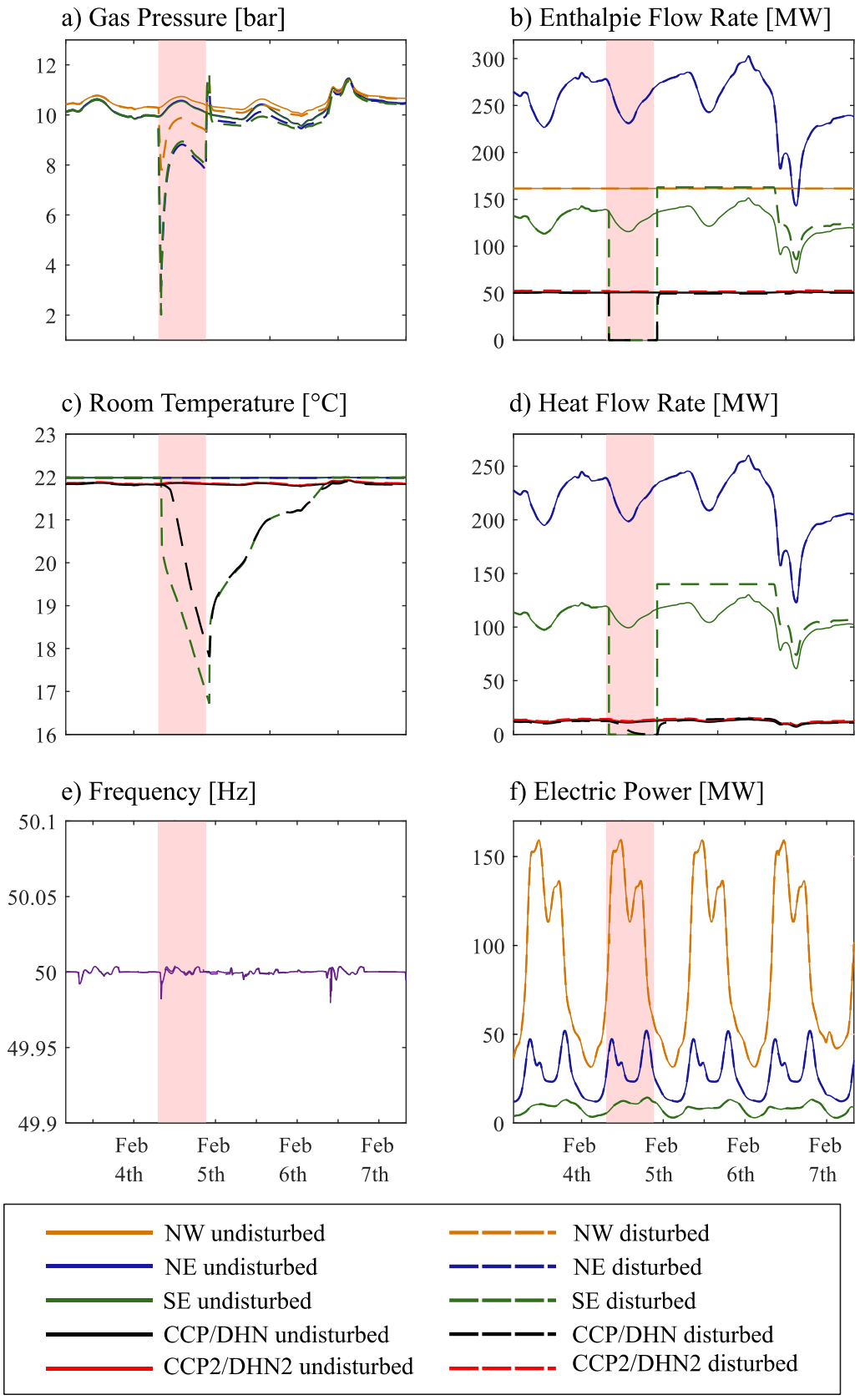

Fig. 10. Simulation results of characteristic values of the gas, heat and power sector for the undisturbed (solid line) and disturbed (dashed line) for RIP 1

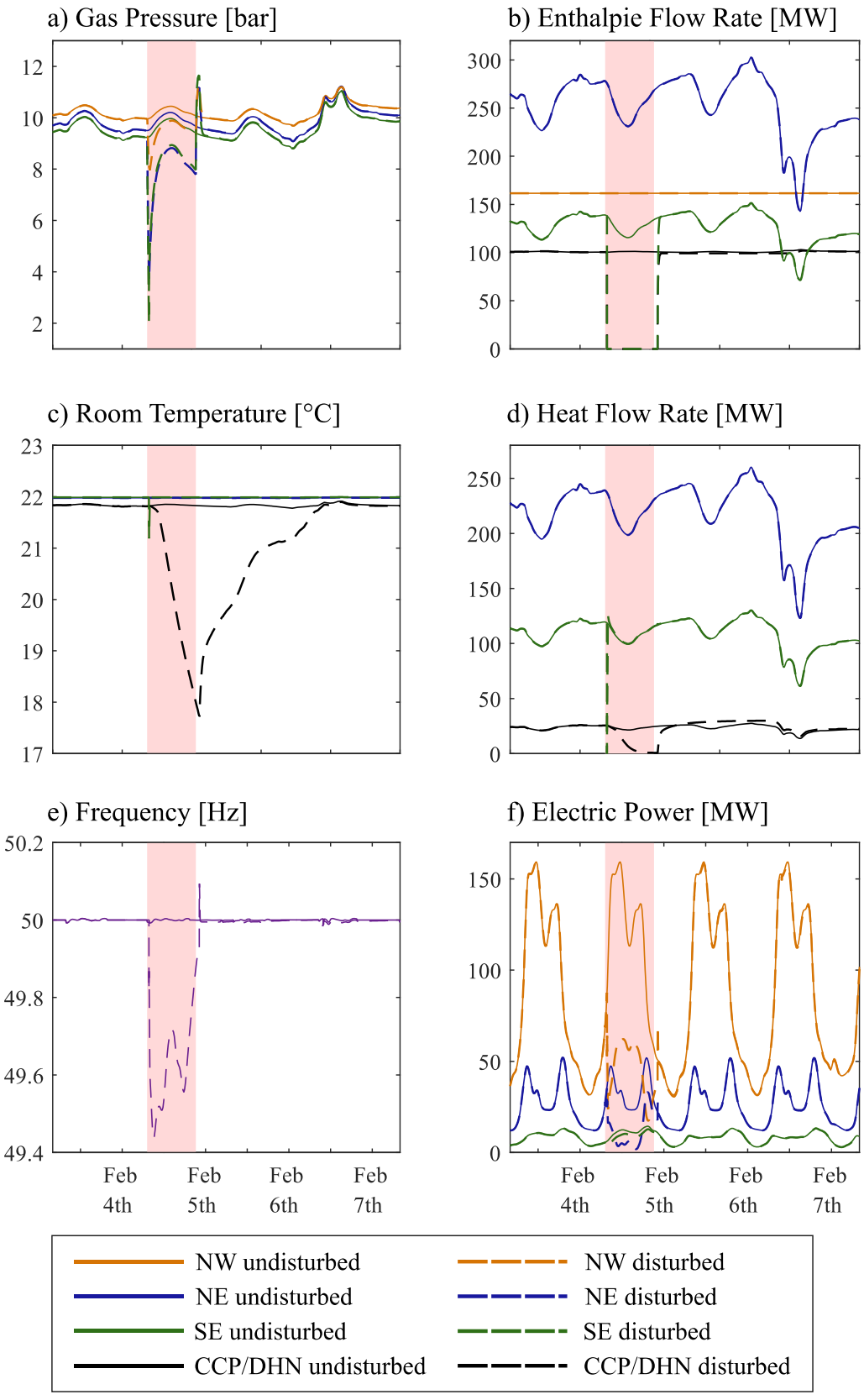

Fig. 11. Simulation results of characteristic values of the gas, heat and power sector for the undisturbed (solid line) and disturbed (dashed line) for RIP 2

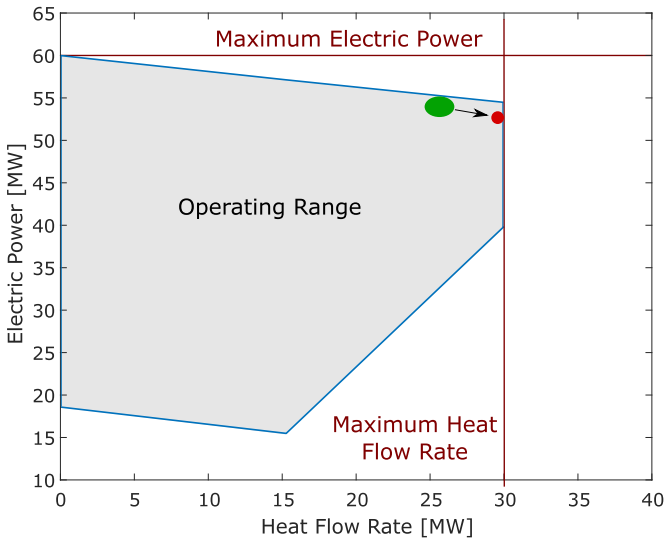

Fig. 12. Shift of the operation point during reheating for the disturbed (red) and the undisturbed system (green)

maintained, since the electric boilers substitute for the shutdown of the gas boilers. Only a short drop occurs in the heat flow rate and the room temperature, due to the reaction time of the control of the electric boiler (Fig. 11, c-d). As with the CCP plant, the DHN is not affected by the electric boiler.

The positive effects in the heating system are accompanied by negative impacts on the power sector. Since the electric grid is not adapted to the new power consumer, the power plants cannot produce enough power to meet the overall demand. Therefore, all consumers are not sufficiently provided with electric power (Fig. 11, f). The huge instability in the grid is also reflected in a drastic drop in the grid frequency (Fig. 11, e).

4.4. Resilience Assessment

Table 2 lists the resilience indices of the three systems. For the gas and heat sector, we chose a tolerance of ±10 %, since these sectors have buffer capacities which can absorb minor disturbances more easily. For the more sensitive power sector, we defined a tolerance band of ±1 %.

The Reference System exhibits the lowest resilience indices for the gas and heat sector, since the heat consumers in particular only depend on one source. The positive effect of several suppliers is noticeable in the power grid. Here, the shutdown of the CCP plant can be compensated by the other power suppliers in the grid, resulting in high resilience indices for all system configurations.

As expected, both intervention plans lead to higher resilience indices in the gas and heat sector, as both introduce an additional energy supplier. However, the positive effects of the implementation of the second CCP for the power sector cannot be derived by comparing its resilience indices since they are all one for the Reference System and RIP 1. Here, a smaller tolerance band or an additional examination of other physical values than grid frequency could help to make the enhanced resilience visible.

It also becomes clear that the effect of the measures on the overall resilience index depends on the amount of affected energy supplied. Therefore, the splitting of the DHN only leads to small gains in the overall resilience index, since only a few consumers benefit.

Another point which must be considered is the effect of the proposed system changes on the overall system. Shifting a sector's failure into another one can cause massive problems in that sector - as the assessment of RIP 2 shows.

The resilience indices for those consumers, which are not negatively affected, are one. Thus, we will only further discuss the resilience indices which are less than one.

Table 2
Resilience indices of consumers and sectors

	NW	NE	SE	CCP/DHN	CCP2/DHN2	Total
			Reference System			
Gas	1.00	1.00	0.16	0.48		0.75
Heat		1.00	0.16	0.34		0.70
Power	1.00	1.00	1.00			1.00
			RIP 1			
Gas	1.00	1.00	0.17	0.50	1.00	0.80
Heat		1.00	0.17	0.35	1.00	0.72
Power	1.00	1.00	1.00			1.00
			RIP 2			
Gas	1.00	1.00	0.50	0.48		0.82
Heat		1.00	1.00	0.34		0.96
Power	0.73	0.74	0.95			0.75

4.5. Reference System

In the Reference System, the CCP plant and the consumers in the southeast and the DHN are not adequately supplied due to the disturbance. For Consumer SE, the resilience indices in the heat and gas sector are the same, since all the gas which is used at this transfer station is burned for heating purposes. Furthermore, there is no additional storage in the heating system, which leads to the analogous behavior in the gas and heat sector which was already described in Section 4.1. This behavior is also described by the identical resilience indices.

The gas which is burned in the CCP plant is used to provide heat and power to its customers. Hence, its resilience index for the gas sector reflects the behavior of its power and heat production. Furthermore, one must bear in mind that the majority of the energy contained in the gas is used to produce power. Therefore, in contrast to Consumer SE, the enthalpy flow rate to the CCP plant does not increase after the disturbance, leading to a resilience index close to 0.5 – one of the cases of the resilience index presented in Section 2.1. Since a buffer storage is installed in the DHN, its heat consumers are supplied with heat for some time, even after the CCP plant is shut down – resulting in a higher resilience index than for the heat consumers in the southeast.

Even though the resilience indices for Consumer SE and the CCP plant and DHN are rather low, the overall resilience indices for the gas and heat sector are 0.75 and 0.70. This is because the undisturbed consumers in the north have the highest share of the overall energy demand, and therefore the biggest influence on the overall resilience index.

The deviations in the power supplied to Consumer NW and NE in the power grid are not reflected by their RI, even though the power curve exceeds the tolerance band. The deviation is so small that it is only expressed by the fourth decimal digit of the resilience index, and is hence negligible.

4.6. Resilience Intervention Plan 1

In RIP 1, the splitting of the DHN leads to a slight delay in the shutdown of the gas boiler in the southeast and the original CCP plant in the east. However, since the delay only lasts 18 minutes, the effect on the resilience index is not significantly reflected by the resilience indices.

Instead, it is noticeable that, due to the normalization, the splitting and resultant reduction of the system considered only has a small impact on the resilience index. Since both the original and the halved DHN/CCP systems are set up similarly and only vary in size, they both react alike, and consequently produce similar resilience indices. The resilience index of the western part of the DHN is one, since it is now supplied by an undisturbed CCP plant.

Since the western DHN and CCP plant are supplied without interruption, the overall resilience indices of the heat and gas sector rise. As the western DHN's share of the overall heat consumption is rather low,

the increase in the heat sector's index is also small. Nevertheless, the western CCP plant's share of the gas demand is higher. Thus, its undisturbed operation has a greater effect on the resilience index of the gas sector.

4.7. Resilience Intervention Plan 2

In RIP 2, the resilience indices of the gas and heat consumers in the southeast rise significantly. Since the electric boilers provide the households with the heat flow rate demanded, their resilience index in the heat sector is one. As this also leads to a shorter reheating phase, the gas enthalpy flow rate is increased for a shorter time period after the disturbance, leading to a higher resilience index for the gas sector as well. Since the enthalpy flow rate to the gas boiler shows a complete shutdown during the disturbance and a quick recovery thereafter, its resilience index is 0.5 – almost like that of the CCP plant. However, the negative effects of this additional power demand on the electric grid are reflected by a much smaller resilience index in the power sector, caused by the insufficient power supply to all three consumers.

5. Conclusions

In this paper, we introduced a resilience assessment method for dynamic simulation results. To do so, we adapted existing methods to fit the specifics of dynamic simulations of integrated energy systems, resulting in a resilience index of between one and zero. We showed the applicability of the resilience index with the aid of an exemplary energy system, which integrated the gas, heat and power sector.

With the resilience index, it is now possible to quantify the resilience of the system considered. In this context, it is possible to "measure" the effectiveness of a system's modification in terms of resilience gains. This makes it possible to compare the system's resilience to other criteria such as sustainability (in terms of CO_2 emissions, for example) or economic efficiency (in terms of operating and/or investment costs).

By assessing not only one energy sector but several interacting sectors, we were able to track "failure shifts" into other sectors, as we demonstrated when evaluating RIP 2. The corresponding resilience indices also reflected this behavior.

By comparing several resilience indices, we were able to locate a system's weak points, for example, the dependence on only one energy supplier in the heat sector of the system presented, and find suitable improvements. In this context, the authors recommend the investigation of different disturbances, especially in other sectors than the gas sector, to gain a better understanding of the system's behavior under stress.

Additionally, the authors would like to stress once more that the presented and assessed energy system was modeled with certain flaws to gain demonstrative results. Therefore, as a next step, the method needs to be applied to an existing energy system.

Moreover, the assessment method presented focuses on the assessment of the resilience in the context of engineering resilience. To gain a broader view of a system's resilience in terms of ecosystem resilience, one must integrate socioecological and technological assessment methods. These two aspects can both correlate as well as compete with each other. For example, the construction of a high-voltage DC-line to gain a higher engineering resilience might raise acceptance as well as rejection, leading to increased or decreased ecological resilience. Implementing both perspectives into an assessment method might lead to a loss of quantifiability, but would allow a more detailed description of a system's resilience, especially to unknown disturbances. The method presented is able to provide important information as part of such a holistic resilience assessment.

Credit Author Statement

Anne Senkel: Conceptualization, Methodology, Software, Visualization, Formal analysis, Writing - Original Draft. **Carsten Bode**: Conceptualization, Methodology, Software, Visualization, Writing - Review & Editing, Funding acquisition. **Gerhard Schmitz**: Conceptualization, Writing - Review and Editing, Supervision, Project administration, Funding acquisition.

Declaration of Competing Interest

The authors declare that they have no known competing financial interests or personal relationships that could have appeared to influence the work reported in this paper.

Acknowledgements

The authors gratefully acknowledge the funding from the German Federal Ministry for Economic Affairs and Energy for the project "ResiliEntEE - Resilienz gekoppelter Energienetze mit hohem Anteil Erneuerbarer Energien" (ResiliEntEE – Resilience of integrated energy networks with a high share of renewable energies, project number: 03ET4048).

References

[1] Allen M, Hd Coninck, Pauline O, Dube Ove Hoegh, Jacob D, et al. Global Warming of 1.5°C: An IPCC special report on the impacts of global warming of 1.5°C above pre-industrial levels and related global greenhouse gas emission pathways, in the context of strengthening the global response to the threat of climate change, sustainable development, and efforts to eradicate poverty. Geneva; 2018.
[2] United Nations Framework Convention on Climate. THE PARIS AGREEMENT. Paris; 2015.
[3] Linkov I, Palma-Oliveira JM. Resilience and Risk: Methods and application in environment, cyber and social domains. Dordrecht: Springer Netherlands; 2017.
[4] Hellige H.D. The Metaphorical Processes in the History of the Resilience Notion and the Rise of the Ecosystem Resilience Theory. In: Ruth M, Gössling-Reisemann S, editors. Handbook on resilience of socio-technical systems. Cheltenham, UK, Northampton, MA: Edward Elgar Publishing; 2019, p. 30–51.
[5] Holling CS. Resilience and Stability of Ecological Systems. Annu. Rev. Ecol. Syst. 1973;4(1):1–23. https://doi.org/10.1146/annurev.es.04.110173.000245.
[6] Gunderson LH, Holling CS. Panarchy: Understanding transformations in human and natural systems. Washington, DC: IslaPress; 2002.
[7] Hosseini S, Barker K, Ramirez-Marquez JE. A review of definitions and measures of system resilience. Reliability Engineering & System Safety 2016;145:47–61. https://doi.org/10.1016/j.ress.2015.08.006.
[8] Gasser P, Lustenberger P, Cinelli M, Kim W, Spada M, Burgherr P, et al. A review on resilience assessment of energy systems. Sustainable and Resilient Infrastructure 2019:1–27. https://doi.org/10.1080/23789689.2019.1610600.
[9] Bruneau M, Chang SE, Eguchi RT, Lee GC, O'Rourke TD, Reinhorn AM, et al. A Framework to Quantitatively Assess and Enhance the Seismic Resilience of Communities. Earthquake Spectra 2003;19(4):733–52. https://doi.org/10.1193/1.1623497.
[10] Cimellaro GP, Reinhorn AM, Bruneau M. Framework for analytical quantification of disaster resilience 2010;32(11):3639–49. https://doi.org/10.1016/j.engstruct.2010.08.008.
[11] Francis R, Bekera B. A metric and frameworks for resilience analysis of engineered and infrastructure systems. Reliability Engineering & System Safety 2014;121:90–103. https://doi.org/10.1016/j.ress.2013.07.004.
[12] Nan C, Sansavini G. A quantitative method for assessing resilience of interdependent infrastructures. Reliability Engineering & System Safety 2017;157:35–53. https://doi.org/10.1016/j.ress.2016.08.013.
[13] Goldbeck N, Angeloudis P, Ochieng WY. Resilience assessment for interdependent urban infrastructure systems using dynamic network flow models. Reliability Engineering & System Safety 2019;188:62–79. https://doi.org/10.1016/j.ress.2019.03.007.
[14] Toroghi SSH, Thomas VM. A framework for the resilience analysis of electric infrastructure systems including temporary generation systems. Reliability Engineering & System Safety 2020;202:107013. https://doi.org/10.1016/j.ress.2020.107013.
[15] Heckel J-P, Becker C. Dynamic Simulation of an Integrated Energy System for Northern Germany with Improved Resilience. editor. In: VDE Verlag, editor. Proceedings of the International ETG Congress; 2019. 2019.
[16] University of Technology Hamburg. TransiEnt Library. [May 12, 2020]; Available from: https://www.tuhh.de/transient-ee/en.
[17] Andresen L , Dubucq P, Peniche Garcia R, Ackermann G, Kather A, Schmitz G. Status of the TransiEnt Library: Transient Simulation of Coupled Energy Networks with High Share of Renewable Energy. In. editor. In: Modelica Association, editor. Proceedings Modelica Conference 2015. Linköping University Electronic Press; 2015. p. 695–705.
[18] Modelica Association. Modelica; Available from: https://www.modelica.org.
[19] Dassault Systèmes. Dymola®; Available from: https://www.3ds.com/de/produkte-und-services/catia/produkte/dymola/.

[20] TLK-Thermo. et al. TILMedia. [March 17, 2020]; Available from: https://www.tlk-thermo.com/index.php/en/software/tilmedia-suite.
[21] VDI - Association of German Engineers. Calculation of transient thermal response of rooms and buildings;91.120.10, 91.140.10(VDI 6007). Berlin. Beuth Verlag GmbH 2015. 06-00.
[22] Lauster M, Mans M, Remmen P, Fuchs M, Müller D. Scalable Design-Driven Parameterization of Reduced Order Models Using Archetype Buildings with Teaser. In: Proceedings of the 6th German-Austrian IBPSA conference; 2016. p. 535–41.
[23] Lange I. Outdoor Temperatures, Hamburg Billwerder, 900s, 2012. [April 21, 2020]; Available from: https://wettermast.uni-hamburg.de/.
[24] European Committee for Standardization. EN. 15251 2012-12, Indoor environmental input parameters for design and assessment of energy performance of buildings addressing indoor air quality, thermal environment, lighting and acoustics;91.140.01. Brüssel; 2007.
[25] Meier H, Fünfgeld C, Adam T, Schieferdecker B. Repräsentative VDEW-Lastprofile. Frankfurt. 1999. Main.
[26] Price WW, Chiang HD, Clark HK, Concordia C, Lee DC, Hsu JC, Ihara S, King CA, Lin CJ, Mansour Y, Srinivasan K, Taylor CW, Vaahedi E. Load representation for dynamic performance analysis (of power systems). IEEE Trans. Power Syst. 1993;8 (2):472–82. https://doi.org/10.1109/59.260837.
[27] Waide P, Brunner C. Energy-Efficiency Policy Opportunities for Electric Motor-Driven Systems. Paris, France; 2011.
[28] Gas Connect Austria. Incident Baumgarten - Chronology. [December 12, 2019]; Available from: https://www.gasconnect.at/en/incident-baumgarten/chronology/.